Effective dynamics of cold atoms flowing in two ring-shaped optical potentials with tunable tunneling

Davit Aghamalyan,[1] Luigi Amico,[1,2] and L. C. Kwek[1,3]
[1]*Centre for Quantum Technologies, National University of Singapore, 3 Science Drive 2, Singapore 117543*
[2]*CNR-MATIS-IMM & Dipartimento di Fisica e Astronomia, Via S. Sofia 64, I-95127 Catania, Italy*
[3]*National Institute of Education and Institute of Advanced Studies, Nanyang Technological University, 1 Nanyang Walk, Singapore 637616*
(Received 6 August 2013; published 13 December 2013)

We study the current dynamics of coupled atomic condensates flowing in two ring-shaped optical potentials. We provide a specific setup where the ring-ring coupling can be tuned in an experimentally feasible way. It is demonstrated that the imaginary time effective action of the system in a weak coupling regime provides a two-level-system dynamics for the phase slip across the two rings. Through two-mode Gross- Pitaevskii mean-field equations, the real-time dynamics of the population imbalance and the phase difference between the two condensates is thoroughly analyzed analytically, as a function of the relevant physical parameters of the system. In particular, we find that the macroscopic quantum self-trapping phenomenon is induced in the system if the flowing currents assume a nonvanishing difference.

DOI: 10.1103/PhysRevA.88.063627 PACS number(s): 03.75.Kk, 42.79.Bh, 45.50.Jf

I. INTRODUCTION

Quantum technology has been leading to realistic applications. To this end, the physical community has been combining ideas and techniques from many fields, including quantum optics, quantum information, and condensed matter physics. Although devising new technological applications remains a defining goal in the field, quantum technologies allow us also to explore new physical regimes, disclosing new fundamental science. Ultracold atoms loaded into optical lattices have been playing an important role in this context [1–9]: They are precise and easily accessible quantum simulators [10], assisting both in the solution of puzzling problems coming from other fields (like solid-state physics) and in the engineering of new quantum phases of extended systems; at the same time, they provide new devices for future technologies, like quantum metrology and quantum computation.

In the scenario depicted above, it is desirable to work with different spatial optical lattice configurations. Ring-shaped optical lattices, in particular, allow us to engineer textbook periodic boundary conditions in many-body systems, and pave the way for exploiting the currents in the lattices as "degrees of freedom" for new quantum devices. Such optical lattices can be generated by employing Laguerre-Gauss laser beams [11,12], by using a rapidly moving laser beam that paints a time-averaged optical dipole potential [13], or by a spatial light modulator (SLM) which imprints a controlled phase onto a collimated laser beam [14]. Light fields of different circular structure have been theoretically proposed [15] by making use of Bessel laser beams. The currents can be generated in several ways: by rotating Bose condensates [16,17], by shining the atoms with electrical fields and making use of so-called synthetic gauge fields [18,19], by using conical-shaped magnetic field [11], or by imprinting a Berry phase [20].

Aside from other applications [21], neutral currents in ring-shaped optical potentials are natural candidates to provide a realization of Josephson junctions flux qubit analog [22,23]. This would exploit the best features of the superconducting flux qubits together with the typically low decoherence time of the cold-atom-based qubits. In Ref. [14] it was evidenced that the program can be indeed realized, constructing the qubit with bosons loaded in single-ring lattice interrupted by a weak link.

In this paper, in contrast, we study a specific device comprising two *homogeneous* ring-shaped potentials with ring-ring coupling. In view of the possible "scalability" of the system, we provide a feasible way to construct a ring-ring interaction, mimicking the inductive coupling in the devices based on charged currents (like before mentioned SQUID-based devices). Indeed, in our specific setup, the coupling can be tuned with simple operations. The system is envisaged to be loaded with bosonic atoms, thus realizing a Bose-Hubbard ladder. We demonstrate that the imaginary-time dynamics of the phase difference across the two weakly coupled rings is controlled by double-well potential. Therefore, the system of two homogenous tunnel-coupled rings indeed defines a qubit. The real-time dynamics is studied within mean-field two-mode Gross-Pitaevskii equations. For the analysis, we benefit from Refs. [24–26]. We demonstrate that the system is characterized by macroscopic quantum self-trapping (MQST) [26–28], the atomic analog of the solid-state polaronic nonlinear self-localization phenomenon due to the strong electron-lattice interaction [24,29]. In contrast to the polaron case, the nonlinearity of the Bose-Einstein condensate self-trapping arises from the many-particle interactions.

The paper is outlined as follows. In Sec. II, we describe the experimental setup realizing two homogenous ring-shaped optical lattices with tunable interaction between them. In Sec. III, we describe how the phase differences along the wells of the two rings can be integrated out in the imaginary time action, this leading to an effective qubit dynamics for the phase difference across the two rings. In Sec. IV, we investigate the real-time dynamics for two coupled ring-shaped optical lattices based on two coupled Gross-Pitaevskii equations, and describe the various possible regimes. In Sec. IV E, regions of oscillations with MQST and phase space diagrams are detailed for the different values of the relevant physical parameters. Finally, we summarize our results in Sec. V.

II. BOSONIC ATOMS LOADED IN TWO-RING OPTICAL POTENTIAL WITH TUNABLE COUPLING

In this section, we describe the experimental setup for realizing two ring-shaped optical lattices with a tunable interaction between them. To achieve the task, we use Laguerre-Gauss (LG) modes to produce closed optical lattices [30,31]. The electric field, with frequency ω, wave vector k, and amplitude E_0, which is propagating along the z axis, can be written in cylindrical coordinates (r,ϕ,z) as $E(r,\phi,z) = E_0 f_{pl}(r) e^{il\phi} e^{i(\omega t - kz)}$, $f_{pl}(r) = (-1)^p \sqrt{\frac{2p!}{\pi(p+|l|)!}} \varepsilon^l L_p^{|l|}(\varepsilon^2) e^{-\varepsilon^2}$, $\varepsilon = \sqrt{2} r/r_0$, where r_0 is the waist of the beam and $L_p^{|l|}$ are associated Laguerre polynomials $L_p^{|l|}(z) = (-1)^m d^m/dx^m [L_{n+m}(z)]$, with $L_{n+m}(z)]$ being the Laguerre polynomials. The numbers p and l label the radial and azimuthal quantum coordinates. In this paper we will consider the case of $p = 0$. We realize an adjustable distance between the two rings by changing the standing wave periodicity in a controllable way [32]: Two beams which are passing through the lens interfere with each other at the focal plane and create interference pattern; the periodicity of the obtained lattice is inversely proportional to the distance between the two beams. The set-up is depicted in Fig. 1. The potential which is obtained at the focal plane of lenses has the following form:

$$V_{\text{latt}} = 4E_0^2 [f_l^2 \cos(k_{\text{LG}} z)^2 + \cos(k_G z)^2 + 2 f_l \cos(k_{\text{LG}} z) \cos(k_G z) \cos(\phi l)], \quad (1)$$

where k_{LG} is the wave vector of the Laguerre-Gauss beam. $k_G = \frac{2\pi D}{\lambda f}$ is the effective wave vector for the Gaussian beams, where D, λ, and f are, respectively, the distance between the two beams passing through the lens, the wavelength of the Gaussian beams, and the focal length of the lens. Using this equation, we can conclude that a stack of closed rings is initially obtained, with $N = l$ lattice sites. The depth of the wells along each ring scales as $\sqrt{1/l!}$. The distance between rings can be controlled by changing the distance between the two Gaussian beams. This can be realized by moving the mirror $M1$. It can be shown that when $k_G = k_{\text{LG}}$, Eq. (1) will give the potential obtained in [11]. So, this potential can be regarded as a generalization of previously obtained potential for the ring-shaped optical lattices. The tunneling matrix element between two rings in the limit $V_0 \gg E_r$, where $V_0 = 4E_0^2$ and $E_r = \frac{\hbar^2 k^2}{2m}$ is the recoil energy, is given by

$$g = 4\sqrt{\frac{\hbar}{\sqrt{2m}}} \frac{V_0^{3/4}}{\sqrt{d}} e^{-\frac{\sqrt{2mV_0}}{\pi\hbar} d}, \quad (2)$$

where $d = \lambda f/D$ is the lattice spacing along z direction. The physical parameters of the set-up are summarized as follows. With a laser intensity of $I = 5\ \text{W/cm}^2$ and the detuning $\Delta = -10^6$ MHz the potential wells are separated by a barrier of $\sim 5\ \mu$K much larger than the chemical potential of a standard condensate (whose temperature can reach few nK). With these parameters the scattering rate is ~ 1 photon/s. It is feasible to have a ring lattice with a radius $r_0 \sim 5\ \mu$m and $N = 20$ lattice sites. With the laser wavelength $\lambda = 830$ nm and lens with $f = 40$ mm the separation between two rings can be adjustable with the setup shown in Fig. 1 in a range of 1.7–6 μm, by changing D from 19.6 to 5.5 mm, whereby the lattice well spacing within each ring is $\sim 1.57\ \mu$m.

Assuming that the particles occupy the lowest Bloch level only (low temperature), both the intra-ring and inter-ring tunneling amplitudes will have a negligible dependence on the ring's radial coordinates.

A single-species bosonic condensate is envisaged to be loaded in the setup described above. Our system is thus governed by a Bose-Hubbard ladder Hamiltonian:

$$H_{\text{BH}} = H_a + H_b + H_{\text{int}} - \sum_{\alpha=a,b} \sum_{i=0}^{N-1} \mu_\alpha \hat{n}_i^\alpha, \quad (3)$$

with

$$H_a = -t \sum_{i=0}^{N-1} (e^{i\Phi_a/N} a_i^\dagger a_{i+1} + \text{H.c.}) + \frac{U}{2} \sum_{i=1}^{N} \hat{n}_i^a (\hat{n}_i^a - 1),$$

$$H_b = -t \sum_{i=0}^{N-1} (e^{i\Phi_b/N} b_i^+ b_{i+1} + \text{H.c.}) + \frac{U}{2} \sum_{i=1}^{N} \hat{n}_i^b (\hat{n}_i^b - 1),$$

$$H_{\text{int}} = -g \sum_{i=0}^{N-1} (a_i^\dagger b_i + b_i^\dagger a_i), \quad (4)$$

where $H_{a,b}$ are the Hamiltonians of the condensates in rings a and b and the H_{int} describes the interaction between rings. Operators $\hat{n}_i^a = a_i^\dagger a_i, \hat{n}_i^b = b_i^\dagger b_i$ are the particle number operators for the lattice site i. Operators a_i and b_i obey the standard bosonic commutation relations. The parameter $t = \int w^{a,b}(\mathbf{x} - \mathbf{x}_i^{a,b})(-\frac{\hbar^2}{2m}\nabla^2 + V_{\text{latt}}) w^{a,b}(\mathbf{x} - \mathbf{x}_i^{a,b})$ is the tunneling rate within lattice neighboring sites (in rings a and b), and $g = \int w^a(\mathbf{x} - \mathbf{x}_i^a)(-\frac{\hbar^2}{2m}\nabla^2 + V_{\text{latt}}) w^b(\mathbf{x} - \mathbf{x}_i^b) d^3\mathbf{x}$ is the tunneling rate between the rings, where $w^{a,b}(\mathbf{x})$ and $\mathbf{x}_i^{a,b}$ are the single-particle Wannier functions and site index for the rings a and b, respectively, and $w^{a,b}(\mathbf{x} - \mathbf{x}_i^{a,b}) = w(x - x_i) w(y - y_i) w(z - z_i \pm d/2)$(where $+$ sign holds for ring a and $-$ sign for ring b), with d being the distance between

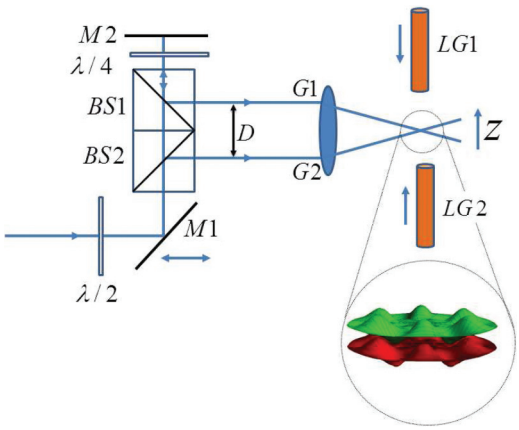

FIG. 1. (Color online) Proposed setup for the ring-ring coupling. Two Gaussian laser beams of wavelength λ and distance D, pass through a lens and interfere in the focal plane (f is the focal length). The distance D can be easily controlled by moving the mirrors. The distance between the fringes is a function of $1/D$ [32]. The resulting Gaussian laser beam with wave vector $k_G = 2\pi D/(\lambda f)$, then, interferes with two counterpropagating Laguerre-Gauss laser beams of amplitude E_0. The inset shows the ring lattice potentials separated by $d = \lambda f/D$. Here $l = 6$ and $p = 0$.

the rings. Here we assume that Wannier functions for the two rings are the same. The repulsion between two atoms on single lattice site is quantified by the on-site interaction matrix element $U = \frac{4\pi a_s \hbar^2}{m} \int |w^{a,b}(\mathbf{x})|^4 d^3\mathbf{x}$, where a_s is the s-wave scattering length of an atom. Finally, the phases Φ_a and Φ_b are the phase twists responsible for the currents flowing along the rings. They can be expressed through vector potential of the so-called synthetic gauge fields in the following way: $\Phi_a/N = \int_{x_i}^{x_{i+1}} \boldsymbol{A(z)} dz$, $\Phi_b/N = \int_{x_i}^{x_{i+1}} \boldsymbol{B(z)} dz$, where $\boldsymbol{A(z)}$ and $\boldsymbol{B(z)}$ are generated vector potentials in rings a and b, respectively (see Appendix A).

III. EFFECTIVE QUBIT DYNAMICS

In this section, we demonstrate that the effective phase dynamics of the system indeed defines a qubit. To this end, we elaborate on the imaginary-time path integral of the partition function of the model Eq. (4) in the limit of large fluctuations of the number of bosons at each site. We first perform a local gauge transformation $a_l \to a_l e^{il\Phi_a}$, $b_l \to b_l e^{il\Phi_b}$, eliminating the contribution of the magnetic field everywhere except at a given site of the ring (twisted boundary conditions [33]). In the regime under scrutiny, the partition function of the model Eq. (4) is [34,35]

$$Z = \mathrm{Tr}(e^{-\beta H_{\mathrm{BH}}}) \propto \int D[\{\phi_i\}] e^{-S[\{\phi_i\}]}, \tag{5}$$

where the effective action is

$$S[\{\phi_i\}] = S_0[\{\phi_i\}] + S_{\mathrm{int}}[\{\phi_i\}], \tag{6}$$

$$S_0[\{\phi_i\}] = \int_0^\beta d\tau \sum_{\substack{i=0 \\ \alpha=\{a,b\}}}^{N-2} \left[\frac{1}{U}(\dot{\phi}_{i,\alpha})^2 - E_J \cos(\phi_{i+1,\alpha} - \phi_{i,\alpha})\right] + \left[\frac{1}{U}(\dot{\phi}_{N-1,\alpha})^2 - E_J \cos(\phi_{0,\alpha} - \phi_{N-1,\alpha} - \Phi_\alpha)\right], \tag{7}$$

$$S_{\mathrm{int}}[\{\phi_i\}] = -E_J' \int_0^\beta d\tau \sum_{i=0}^{N-1} \cos\left(\phi_{i,a} - \phi_{i,b} - \frac{\Phi_a - \Phi_b}{N} i\right), \tag{8}$$

with $E_J = t\langle n\rangle$ and $E_J' = g\langle n\rangle$.

Because of the gauge transformations, the phase slip is produced only at the boundary. We define $\theta_\alpha \doteq \phi_{N-1,\alpha} - \phi_{0,\alpha}$. The goal now is to integrate out the phase variables in the bulk. Assuming that the two rings are weakly coupled and that $U/E_J \ll 1$, the bulk variables are not involved in the inter-ring tunneling term because we can take $\phi_{i,a} \approx \phi_{i,b}$ everywhere except at the boundary:

$$\sum_{i=0}^{N-1} \cos\left(\phi_{i,a} - \phi_{i,b} - \frac{\Phi_a - \Phi_b}{N} i\right) = \sum_{i=0}^{N-2} \cos\left(\frac{\Phi_a - \Phi_b}{N} i\right) + \cos\left(\theta_a - \theta_b - \frac{\Phi_a - \Phi_b}{N}(N-1)\right), \tag{9}$$

where, without loss of generality, we can assume $\phi_{0,a} \equiv \phi_{0,b}$. Therefore the nontrivial path integration corresponds to $S_0[\{\phi_i\}]$ only. To achieve the task we observe that in the phase-slips-free sites the phase differences are small, so the harmonic approximation can be applied:

$$\sum_{i=0}^{N-1} \cos(\phi_{i+1,\alpha} - \phi_{i,\alpha}) \mapsto \cos(\theta_\alpha - \Phi_\alpha) - \sum_{i=0}^{N-2} \frac{(\phi_{i+1,\alpha} - \phi_{i,\alpha})^2}{2}. \tag{10}$$

In order to facilitate the integration in the bulk phases, we express the single $\phi_{0,\alpha}$ and $\phi_{N-1,\alpha}$ as $\phi_{0,\alpha} = \tilde{\phi}_{0,\alpha} + \theta_\alpha/2$, $\phi_{N-1,\alpha} = \tilde{\phi}_{0,\alpha} - \theta_\alpha/2$. We observe that the sum of the quadratic terms above involves $N-1$ fields with periodic boundary conditions: $\{\tilde{\phi}_{0,\alpha}, \phi_{1,\alpha}, \ldots, \phi_{N-2,\alpha}\} \equiv \{\psi_{0,\alpha}, \psi_{1,\alpha}, \ldots, \psi_{N-2,\alpha}\}$, $\psi_{N-1,\alpha} = \psi_{0,\alpha}$. Therefore,

$$\sum_{i=0}^{N-2} (\phi_{i+1,\alpha} - \phi_{i,\alpha})^2 = \sum_{i=0}^{N-2} (\psi_{i+1,\alpha} - \psi_{i,\alpha})^2 + \frac{1}{2}\theta_\alpha^2 + \theta_\alpha(\psi_{N-2,\alpha} - \psi_{1,\alpha}). \tag{11}$$

The effective action, $S_0[\{\phi_i\}]$, can be split into two terms $S_0[\{\phi_i\}] = S_{01}[\theta_\alpha] + S_{02}[\{\psi_{i\alpha}\}]$ with

$$S_{01}[\theta_\alpha] = \int_0^\beta d\tau \left[\frac{1}{U}(\dot{\theta}_\alpha)^2 + \frac{E_J}{2}\theta_\alpha^2 - E_J \cos(\theta_\alpha - \Phi_\alpha)\right], \tag{12}$$

$$S_{02}[\{\psi_{i,\alpha}\}, \theta_\alpha] = \int_0^\beta d\tau \left\{\frac{1}{U}(\dot{\psi}_{0,\alpha})^2 + \sum_{i=0}^{N-2}\left[\frac{1}{U}(\dot{\psi}_{i,\alpha})^2 + \frac{E_J}{2}(\psi_{i+1,\alpha} - \psi_{i,\alpha})^2\right] + E_J\theta_\alpha(\psi_{N-2,\alpha} - \psi_{1,\alpha})\right\}. \tag{13}$$

The integration of the fields $\psi_{i,\alpha}$ proceeds according to the standard methods (see [36]). The fields that need to be integrated out are expanded in Fourier series (N is assumed to be even): $\psi_{l,\alpha} = \frac{1}{\sqrt{N-1}}[\psi_{0,\alpha} + (-)^l \psi_{N/2,\alpha} + \sum_{k=1}^{(N-2)/2}(\psi_{k,\alpha} e^{\frac{2\pi i k l}{N-1}} + \text{c.c.})]$, with $\psi_{k,\alpha} = a_{k,\alpha} + i b_{k,\alpha}$. The coupling term in Eq. (13) involves only the imaginary part of $\psi_{k,\alpha}$: $\psi_{N-2,\alpha} - \psi_{1,\alpha} = \sum_k b_{k,\alpha}\zeta_k$, being $\zeta_k = \frac{4}{\sqrt{N-1}} \sin(\frac{2\pi k}{N-1})$. Therefore,

$$S_{02}[\{\psi_{i,\alpha}\}, \theta_\alpha] = \int_0^\beta d\tau \frac{1}{U} \sum_k \left[(\dot{a}_{k,\alpha})^2 + \omega_k^2 a_{k,\alpha}^2\right] + \int_0^\beta d\tau \frac{1}{U} \sum_k \left[(\dot{b}_{k,\alpha})^2 + \omega_k^2 b_{k,\alpha}^2 + E_J U \zeta_k \theta_\alpha b_{k,\alpha}\right], \tag{14}$$

where $\omega_k = \sqrt{2E_J U[1 - \cos(\frac{2\pi k}{N-1})]}$. The integral in $\{a_{k,\alpha}\}$ leads to a Gaussian path integral; It does not contain the interaction with θ_α, and therefore brings a prefactor multiplying the effective action, that does not affect the dynamics. The

integral in $\{b_{k,\alpha}\}$ involves the interaction and therefore leads to a nonlocal kernel in the imaginary time: $\int d\tau d\tau' \theta_\alpha(\tau) G(\tau - \tau')\theta_\alpha(\tau')$. The explicit form of $G(\tau - \tau')$ is obtained by expanding $\{b_{k,\alpha}\}$ and θ_α in Matsubara frequencies ω_l. The corresponding Gaussian integral yields to

$$\int D[b_{k,\alpha}] e^{-\int_0^\beta d\tau S_{02}} \propto \exp\left(- \beta U E_J^2 \sum_{l=0}^{\infty} \tilde{Y}(\omega_l)|\theta_l|^2 \right), \tag{15}$$

with $\tilde{Y}(\omega_l) = \sum_{k=1}^{(N-2)/2} \frac{\zeta_k^2}{\omega_k^2 + \omega_l^2}$. The $\tau = \tau'$ term is extracted by summing and subtracting $\tilde{Y}(\omega_l = 0)$; this compensates the second term in Eq. (12).

The effective action finally reads as

$$S_{\text{eff}} = \int_0^\beta d\tau \left[\frac{1}{2U} \sum_{\alpha=a,b} \dot{\theta}_\alpha^2 + U(\theta_a, \theta_b) \right] - \frac{E_J}{2U(N-1)} \sum_{\alpha=a,b} \int_0^\beta d\tau d\tau' \theta_\alpha(\tau) G_\alpha(\tau - \tau') \theta_\alpha(\tau'), \tag{16}$$

where

$$U(\theta_a, \theta_b) \doteq \sum_{\alpha=a,b} \left[\frac{E_J}{2(N-1)} (\theta_\alpha - \Phi_\alpha)^2 - E_J \cos(\theta_\alpha) \right] - E_J' \cos\left[\theta_a - \theta_b - \frac{N-2}{N} (\Phi_a - \Phi_b) \right]. \tag{17}$$

We observe that for large N, the potential $U(\theta_a, \theta_b)$ provides the effective phase dynamics of Josephson junctions flux qubits realized by Mooij *et al.* (large N corresponds to large geometrical inductance of flux qubit devices) [22]. In that article, the landscape was thoroughly analyzed. The qubit is realized by superposing the two states $|\theta_1\rangle$ and $|\theta_2\rangle$ corresponding to the minima of $U(\theta_a, \theta_b)$. The degeneracy point is achieved at $\Phi_b - \Phi_a = \pi$ (see Fig. 2). We comment that the ratio E_J'/E_J controls the relative size of the energy barriers between minima intra- and minima inter-"unit cells" of the (θ_a, θ_b) phase space, and therefore is important for designing the qubit. In our system E_J'/E_J can be fine tuned with the scheme shown in Fig. 1. The kernel in the nonlocal term is given by $G_a(\tau) = G_b(\tau) = G(\tau)$, with

$$G(\tau) = \sum_{l=0}^{\infty} \sum_{k=1}^{\frac{N-2}{2}} \frac{\omega_l^2 \left(1 + \cos\left[\frac{2\pi k}{N-1}\right]\right)}{2E_J U \left(1 - \cos\left[\frac{2\pi k}{N-1}\right]\right) + \omega_l^2} e^{i\omega_l \tau}. \tag{18}$$

The external bath vanishes in the thermodynamic limit and the effective action reduces to the Caldeira-Leggett one [36,37].

IV. REAL-TIME DYNAMICS: TWO COUPLED GROSS-PITAEVSKII EQUATIONS

In this section we study the dynamics of the number and phase imbalance of two bose condensates confined in the ring-shaped potential. For this goal, we assume that the system described by a Bose-Hubbard ladder Eq. (4), is in a superfluid regime, with negligible quantum fluctuations. The order parameters can be defined as the expectation values of

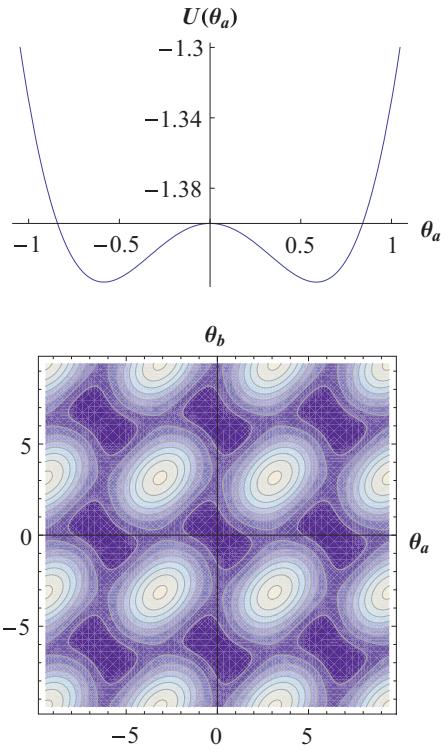

FIG. 2. (Color online) (Top) The effective potential landscape. (Bottom) The double well for $\theta_a = -\theta_b$. The parameters are $E_J'/E_J = 0.8$ and $\Phi_a - \Phi_b = \pi$.

boson operators in the Heisenberg picture:

$$\varphi_{a,i}(s) = \langle a_i(s) \rangle, \varphi_{b,i}(s) = \langle b_i(s) \rangle, \tag{19}$$

implying that the Heisenberg equations for the operators a_i and b_i are simplified into the Gross-Pitaevskii equations for the corresponding expectation values:

$$i\hbar \frac{\partial \varphi_{a,i}}{\partial s} = -t(e^{i\Phi_a/N} \varphi_{a,i+1} + e^{-i\Phi_a/N} \varphi_{a,i-1}) + U|\varphi_{a,i}|^2 \varphi_{a,i} - \mu_a \varphi_{a,i} - g\varphi_{b,i}, \tag{20}$$

$$i\hbar \frac{\partial \varphi_{b,i}}{\partial s} = -t(e^{i\Phi_b/N} \varphi_{b,i+1} + e^{-i\Phi_b/N} \varphi_{b,i-1}) + U|\varphi_{b,i}|^2 \varphi_{b,i} - \mu_b \varphi_{b,i} - g\varphi_{a,i}. \tag{21}$$

We assume that $\varphi_{a,i+1} - \varphi_{a,i} = \frac{\varphi_a(s)}{\sqrt{N}}$ and $\varphi_{b,i+1} - \varphi_{b,i} = \frac{\varphi_b(s)}{\sqrt{N}}$ for all $i, j = 0, .., N$, where N is a total number of ring-lattice sites. From Eqs. (20) and (21) we obtain

$$i\hbar \frac{\partial \varphi_a}{\partial s} = -2t \cos(\Phi_a/N) \varphi_a + \frac{U}{N} |\varphi_a|^2 \varphi_a - \mu_a \varphi_a - g\varphi_b, \tag{22}$$

$$i\hbar \frac{\partial \varphi_b}{\partial s} = -2t \cos(\Phi_b/N) \varphi_b + \frac{U}{N} |\varphi_b|^2 \varphi_b - \mu_b \varphi_b - g\varphi_a. \tag{23}$$

Employing the standard phase-number representation, $\varphi_{a,b} = \sqrt{N_{a,b}} e^{i\theta_{a,b}}$, two pairs of equations are obtained for imaginary

and real parts:

$$\hbar\frac{\partial N_a}{\partial s} = -2g\sqrt{N_a N_b}\sin(\theta_b-\theta_a),$$
$$\hbar\frac{\partial N_b}{\partial s} = 2g\sqrt{N_a N_b}\sin(\theta_b-\theta_a), \tag{24}$$

$$\hbar\frac{\partial\theta_a}{\partial s} = -2t\cos\Phi_a/N - \frac{UN_a}{N} + \mu_a + g\sqrt{\frac{N_b}{N_a}}\cos(\theta_b-\theta_a),$$
$$\hbar\frac{\partial\theta_b}{\partial s} = -2t\cos\Phi_b/N - \frac{UN_b}{N} + \mu_b + g\sqrt{\frac{N_a}{N_b}}\cos(\theta_b-\theta_a). \tag{25}$$

From Eq. (24) it results that $\frac{\partial N_a}{\partial s}+\frac{\partial N_b}{\partial s}=0$, reflecting the conservation of the total bosonic number $N_T = N_a + N_b$. From Eqs. (24) and (25) we get

$$\frac{\partial Z}{\partial\tilde{s}} = -\sqrt{1-Z^2}\sin\Theta, \tag{26}$$

$$\frac{\partial\Theta}{\partial\tilde{s}} = \Delta + \lambda\rho Z + \frac{Z}{\sqrt{1-Z^2}}\cos\Theta, \tag{27}$$

where we introduced new variables: the dimensionless time $2gs/\hbar\to\tilde{s}$, the population imbalance $Z(\tilde{s}) = (N_b - N_a)/(N_a+N_b)$, and the phase difference between the two condensates $\Theta(\tilde{s}) = \theta_a - \theta_b$. It is convenient to characterize the system with a new set of parameters: external driving force $\Delta = (2t(\cos\Phi_a/N - \cos\Phi_b/N) + \mu_b - \mu_a)/2g$, the effective scattering wavelength $\lambda = U/2g$, and the total bosonic density $\rho = N_T/N$. The exact solutions of Eqs. (26) and (27) in terms of elliptic functions [26] can be adapted to our case and it is detailed in Appendix A. As it has been noticed in [26] equations can be derived as Hamilton equations with

$$H(Z(\tilde{s}),\Theta(\tilde{s})) = \frac{\lambda\rho Z^2}{2} + \Delta Z - \sqrt{1-Z^2}\cos\Theta, \tag{28}$$

by considering Z and Θ as conjugate variables. Since the energy of the system is conserved, $H(Z(\tilde{s}),\Theta(\tilde{s})) = H(Z(0),\Theta(0)) = H_0$.

The dynamics can be visualized with the help of the mechanical system provided by a rotator of length of $\sqrt{1-Z^2}$ driven by the external force Δ. In this picture, Z is considered to be an angular momentum of the rotator and $\lambda\rho$ its moment of inertia. For $\Delta = 0$, the dynamics of the rotator depends on the value of initial angular momentum $Z(0)$. For small initial kinetic energy $\frac{\lambda\rho Z(0)^2}{2}$, the rotator makes small oscillations and its trajectory is an opened curve, thus $\langle Z\rangle = 0$. For the critical value Z_c the rotator reaches the equilibrium vertical position corresponding to $\phi=\pi$. For $Z_0 > Z_c$ the rotator performs revolutions around his fixed point with $\Delta\theta = 2\pi$ and $\langle Z\rangle = 0$. In the case of nonvanishing Δ, the dynamics of the rotator depends on $Z(0)$ and external force Δ. Because of the Δ, the system oscillates around a shifted equilibrium value (which leads to an asymmetry into the system) and $\langle Z\rangle \neq 0$ for all the cases.

Below, we discuss the different regimes for population imbalance, emerging from Eqs. (26) and (27) depending on the values of parameters $\lambda\rho$ and Z_0 (see Appendix A for technical details). For each physical regime we further discuss the solution for both cases of vanishing and nonvanishing Δ.

A. Population imbalance and oscillation frequencies for $\lambda\rho = 0$

(I-A.) $\Delta = 0$. For noninteracting atoms, the solution of Eqs. (26) and (27) is

$$Z(\tilde{s}) = \sqrt{1-H_0^2}\sin(\tilde{s}+\tilde{s}_0), \tag{29}$$

where $\tilde{s}_0 = \arcsin\frac{Z_0}{\sqrt{1-H_0^2}}$ and $H_0 = -\sqrt{1-Z_0^2}\cos\Theta_0$ is an initial energy of the system. Equation (29) describes sinusoidal Rabi oscillations between the two traps with frequency $\omega_0 = 2g$. These oscillations are equivalent to single atom dynamics, rather than a Josephson effect arising from the interacting superfluid condensate.

(II-A.) $\Delta\neq 0$. Depending on the value of the determinant $D = 1 - H_0^2/(\Delta^2+1)$ of the equation $f(Z) = -(\Delta^2+1)Z^2 + 2H_0\Delta Z + 1 - H_0^2$, the population imbalance is either oscillating around a nonzero average, reflecting the MQST phenomenon, or staying constant in time. A numerical analysis shows that $D\geqslant 0$. Therefore, there are two different subcases. When $D=0$ (which can be satisfied only if $\sin\Theta_0 = 0$), the population imbalance stays constant and takes on the value,

$$Z = Z_0 = -\frac{\Delta}{\sqrt{1+\Delta^2}} = \text{const}. \tag{30}$$

For this value of the initial population imbalance, $\Theta = \text{const}$. In the case when $D>0$, the subsequent expression for $Z(t)$ is obtained:

$$Z(\tilde{s}) = B - \frac{C}{A}\sin[a(\tilde{s}-\tilde{s}_0)], \tag{31}$$

where $\tilde{s}_0 = \frac{1}{A}\arcsin[\frac{A}{C}(Z_0-B)], A = \sqrt{1+\Delta^2}, B = \frac{\Delta H_0}{A^2}$, and $C = \sqrt{1-\frac{H_0^2}{A^2}}$. As it is seen from Eq. (31), the system is oscillating about a nonzero average value B with frequency,

$$\omega = \omega_0\sqrt{1+\Delta^2}. \tag{32}$$

All the regimes discussed for this case are displayed in Fig. 3.

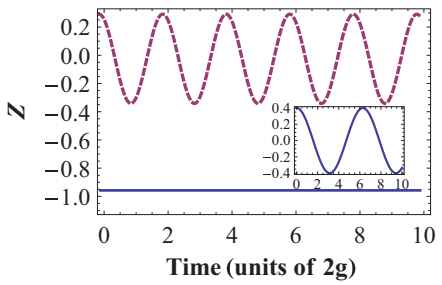

FIG. 3. (Color online) The population imbalance in two coupled rings for the case $\lambda\rho = 0$. Solid and dashed lines correspond to the cases $D=0$ and $D>0$ accordingly in the regime of nonzero Δ. An inset shows behavior of $Z(\tilde{s})$ for vanishing Δ. Here $\lambda\rho = 0$, $\Delta = 2$, $\Theta_0 = 0$ implying that $\omega\simeq 3.16\omega_0$.

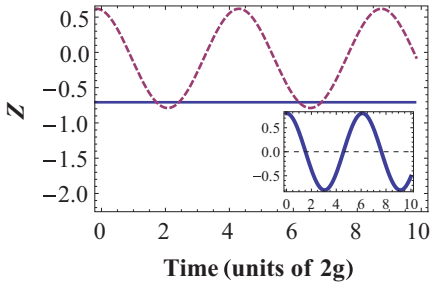

FIG. 4. (Color online) The population imbalance in two coupled rings for the case $\lambda\rho \ll 1$. Solid and dashed lines correspond to the cases $\delta = 0$ and $\delta < 0$ accordingly in the regime of nonzero Δ. An inset shows behavior of $Z(\tilde{s})$ for the vanishing Δ. Here $\lambda\rho = 0.1$, $\Theta_0 = 0$, and $\Delta = 1$.

B. Population imbalance and oscillation frequencies in the limit $\lambda\rho \ll 1$

(I-B.) $\Delta = 0$. The qualitative behavior of the dynamics for this subcase depends on the elliptic modulus k which is given by Eq. (B8). For $\lambda\rho \ll 1$,

$$k = Z(0)\lambda\rho\left(1 - \frac{\lambda\rho}{2}\sqrt{1 - Z(0)^2}\right). \tag{33}$$

So $k \sim 0$ and therefore $Z(t)$ displays only one regime given by

$$Z(\tilde{s}) \simeq Z(0)(\cos\omega(\tilde{s} - \tilde{s}_0) + \frac{k}{4}(\omega(\tilde{s} - \tilde{s}_0) - \sin 2\omega(\tilde{s} - \tilde{s}_0)) \times \sin\omega(\tilde{s} - \tilde{s}_0)), \tag{34}$$

where $\omega \simeq 2g(1 + \frac{\lambda}{2}\rho\sqrt{1 - Z(0)^2})$ and $\tilde{s}_0$ is fixing initial condition. Therefore, in this regime the population imbalance is characterized by almost sinusoidal oscillations about zero average (see the inset of Fig. 4).

(II-B.) $\Delta \neq 0$. In this case behavior of $Z(t)$ is governed by determinant δ of the cubic equation Eq. (B15). There are two different regimes depending on the initial value of the population imbalance which are given by the value of δ. All the regimes can be discussed by expressing the Weierstrass function in Eq. (B11) using Jacobian elliptic functions. In the

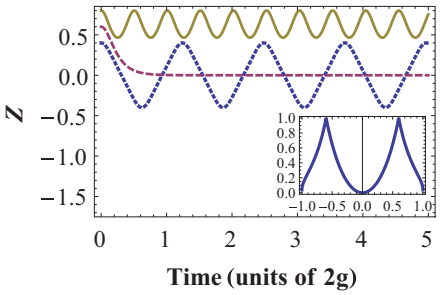

FIG. 5. (Color online) The population imbalance in two coupled rings for the intermediate value of $\lambda\rho$ and $\Delta = 0$. Dotted line, dashed line, and solid line, respectively, correspond to the cases $k < 1, k = 1, k > 1$. Inset shows dependence of the elliptic modulus $\tilde{k}$ ($\tilde{k} = k$ for $k < 1$; 1 for $k = 1$; and $1/k$ for $k > 1$) from the value of Z_0. Here $\lambda\rho = 10$, $\Theta_0 = 0$.

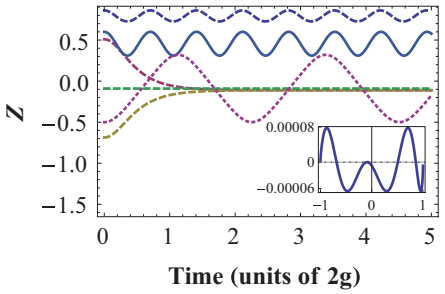

FIG. 6. (Color online) The population imbalance in two coupled rings for the intermediate value of $\lambda\rho$ and $\Delta = 1$. Dotted line, dashed line, and solid line, respectively, correspond to the cases $\delta < 0, \delta = 0, \delta > 0$. Inset shows dependence of determinant δ of the characteristic cubic equation from the value of Z_0. Here $\lambda\rho = 10$, $\Theta_0 = 0$.

limit of $\delta = 0$, the population imbalance takes the form,

$$Z(\tilde{s}) = Z(0) + \frac{f'[Z(0)]/4}{-c + 3c\left[\sin\left(-\sqrt{3c}\frac{\lambda\rho}{2}\tilde{s}\right)\right]^{-2} - f''[Z(0)]/24}. \tag{35}$$

For the parameters discussed in the article, $f'[Z(0)] \sim 10^{-14}$; so the population imbalance is staying constant due to the same reason as for the subcase $D = 0$ of the previous section. In the limit of $\delta < 0$, the population imbalance takes the form,

$$Z(\tilde{s}) = Z(0) + \frac{f'[Z(0)]/4}{e_2 + H_2\frac{1+\cos(\lambda\rho\sqrt{H_2}\tilde{s})}{1-\cos(\lambda\rho\sqrt{H_2}\tilde{s})} - f''[Z(0)]/24}, \tag{36}$$

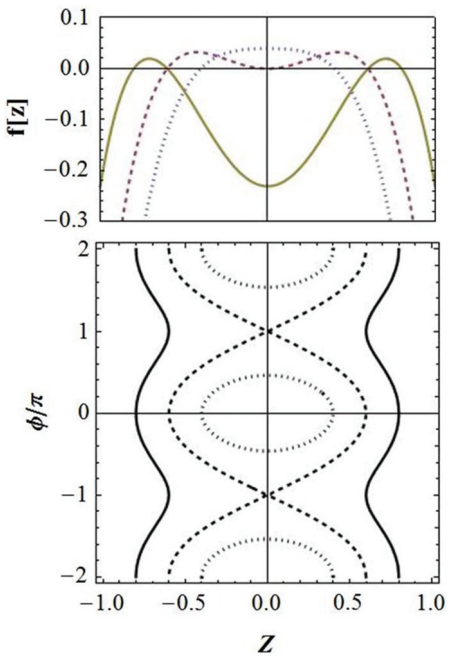

FIG. 7. (Color online) Dependence of the characteristic function $f(Z)$ on population imbalance (top) and phase space diagram (bottom) for the case $\Delta = 0$. Oscillations can occur only in the regions where $f(Z) \geqslant 0$. Dotted, dashed, and solid lines, respectively, correspond to the values $Z_0 = 0.4, 0.6, 0.8$ (for these values $k < 1, k = 1$, and $k > 1$, respectively). Here $\Theta_0 = 0$ and $\lambda\rho = 10$.

where $e2, H_2$ are defined in Appendix A. Equation (36) is correct when $1/2 - 3e_2/4H_2 \simeq 0$ (for the parameters considered in the article $m \simeq 10^{-7}$).

As one can see from this formula, the population imbalance is oscillating about nonzero average (MQST regime) with frequency given by

$$\omega = 2g\left(\sqrt{1+\Delta^2} + \frac{(Z(0)\Delta - \sqrt{1-Z(0)^2})(2\Delta^2-1)}{2(1+\Delta^2)^{3/2}}\lambda\rho\right). \tag{37}$$

This two regimes are shown in Fig. 4.

C. Population imbalance and oscillation frequencies for the intermediate values of $\lambda\rho$

(I-C.) $\Delta = 0$. The population imbalance can be expressed in terms of Jacobi functions "cn" and "dn" [Eq. (B7)] and behavior of the solutions (which is summarized in Fig. 5) is governed by elliptic modulus k [Eq. (B8)].

(II-C.) $\Delta \neq 0$. The population imbalance can be written in terms of Weierstrass elliptic function [Eq. (B11)] behavior of the solutions is governed by determinant δ [Eq. (B15)] of the characteristic cubic equation. The dynamics for this subcase is given by Fig. 6. In both cases oscillation periods can be expressed in terms of elliptic integral of the first kind [Eqs. (B10) and (B20)]. When $\delta = 0$ oscillations are exponentially suppressed or there are sinusoidal oscillations depending on the relative sign between $g2$ and $g3$ [Eqs. (B16) and (B17)]. Because it is possible to express Weierstrass function through Jacobian functions "sn" and "cn" [Eqs. (B18) and (B19)] we are coming to conclusion that in general population imbalance can be written in terms of Jacobian functions.

D. Population imbalance and oscillation frequencies for $\lambda\rho \to \infty$

In analogy to a nonrigid pendulum, it is expected that in this regime, no oscillations occur and the population imbalance stays constant: The parameter $\lambda\rho$ is playing the role of the moment of inertia and when it is very big it is not possible to force the pendulum to rotate by providing it with a finite amount of angular momentum (which is Z_0) or by acting on it with finite driving force Δ. It is also possible to arrive at this conclusion from the analytical solutions shown in Appendix A.

(I-D.) $\Delta = 0$. We see that $k \to \infty$ and $Z(\tilde{s}) = Cdn[(C\lambda\rho/k(\tilde{s} - \tilde{s}_0),0) = Z_0 = \text{const}]$.

(II-D.) $\Delta \neq 0$. In this case $\delta = 0$ and the solution is given by Eq. (B17). But because in this limit $f'(Z_1) \to 0$ and $Z_1 = Z_0$ we conclude that $Z(\tilde{s}) = Z_0 = \text{const}$.

E. MQST and phase space diagrams

In this section, it is shown how it is possible to find the values of the population imbalance which takes the system and the regions of MQST depending on Z_0. The phase diagrams in the $\Theta/\pi, Z(\tilde{s})$ space for the cases of zero and nonzero values of the Δ are introduced as well.

As it is seen from Eq. (B5), if the characteristic quartic equation [which is given be Eq. (B6)] $f(Z) < 0$, then the time takes imaginary values. So we conclude that allowed regions of $Z(\tilde{s})$ are given by the condition,

$$f(Z) \geqslant 0, \tag{38}$$

Eq. (B4), derived from the Gross-Pitaevskii Eqs. (26) and (27), can be written as an equation of motion of a classical particle with a coordinate Z, potential energy $U(Z)$, and total energy E:

$$\dot{Z}^2(\tilde{s}) + U(Z) = E, \tag{39}$$

where the first term is playing the role of kinetic energy. The second term and the total energy are given by

$$\begin{aligned} U(Z) &= Z^2\left(\frac{(\lambda\rho)^2 Z^2}{4} + 1 + \Delta^2 - H_0\lambda\rho\right) \\ &\quad + Z(\lambda\rho\Delta Z^2 - 2H_0\Delta) \\ E &= \dot{Z}^2(0) + U(Z(0)) = 1 - H_0^2. \end{aligned} \tag{40}$$

Within the classical mechanics analogy, $f(Z)$ plays the role of $E - U$. The motion of the particle lies within the regions of the classical turning points in which the total energy equals to the potential energy. So Eq. (38) has a simple physical meaning: Classical particle can only move in the regions where total energy is equal or bigger than potential energy. From the upper graphs of Figs. 7 and 8, one can see that when all values of parameters are fixed, and we start to change the value of Z_0 then the function $f(Z)$ changes from parabolic to double well.

When $\Delta = 0$ then for the parabolic potential $Z(\tilde{s})$ oscillates about an average of zero value, and when $Z(0) > Z_c$ ($Z_c = 0.6$ in our case) the particle is forced to oscillate about a nonzero average in one of the two wells as it is seen from Fig. 7 which is evidence of the MQST. Indeed such a phenomenon occurs in the system for $Z(0) > Z_c$, where

$$Z_c = \pm\sqrt{\frac{2}{\lambda\rho} - \frac{1+\cos 2\Theta_0}{(\lambda\rho)^2} + \frac{\sqrt{(1+\cos 2\Theta_0)(\cos 2\Theta_0 + 2(\lambda\rho-1)^2 - 1)}}{(\lambda\rho)^2}}, \tag{41}$$

which reduces to

$$Z_c = \pm 2\frac{\sqrt{\lambda\rho - 1}}{\lambda\rho} \tag{42}$$

for $\sin\Theta_0 = 0$. For the $Z_0 = Z_c$, the particle moves from Z_0 to the point $Z = 0$ where it stays for an infinite time because at this point $f'(Z) = 0$ which means there is no force acting on the particle [$U'(Z) = 0$].

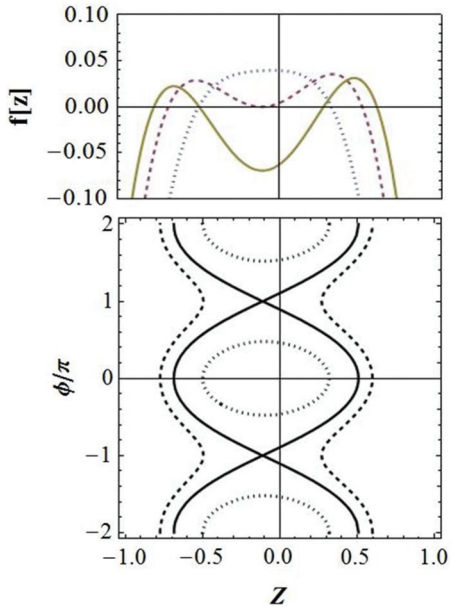

FIG. 8. (Color online) Dependence of the characteristic function $f(Z)$ on population imbalance (top) and phase space diagram (bottom) for the case $\Delta \neq 0$. Oscillations can occur only in the regions where $f(Z) \geqslant 0$. Dotted, dashed, and solid lines, respectively, correspond to the values $Z_0 = -0.5, 0.509117, 0.6$ (for these values $\delta < 0, \delta = 0$, and $\delta > 0$, respectively). Here $\Theta_0 = 0$ and $\lambda\rho = 10$.

When $\Delta \neq 0$, all the regimes are the same but with the difference that the external force Δ breaks the symmetry at the point $Z = 0$, with the following two consequences: (1) $Z(\tilde{s})$ is always oscillating about a nonzero average, and (2) for the critical value Z_c, the oscillations are damping to the nonzero value of population imbalance as one can see from Fig. 8. So for the all values of Z_0 (excepting the values for which $\delta = 0$) the effect of MQST occurs in the system.

The lower graphs of Figs. 7 and 8 display corresponding phase versus population imbalance. After expressing the phase using the population imbalance from Eq. (28), we get

$$\Theta = \arccos\left[\frac{H_0 - \frac{\lambda\rho Z^2}{2} - \Delta Z}{\sqrt{1-Z^2}}\right]. \tag{43}$$

From Fig. 7 it is seen that when $Z < Z_c$, the phase diagram is a closed curve and the phase is oscillating about zero average value. At the critical point, the phase diagram starts to split into the two open curves and for $Z > Z_c$ it consists of two open curves and the phase takes any value in the interval $[-\infty, \infty]$. In the case when $\Delta \neq 0$ the phase diagram is changing depending on Z_0 in a similar way but with the difference that the external force Δ is breaking the symmetry about the origin of Z axis as demonstrated in Fig. 8.

V. CONCLUSIONS

In this paper, we study the dynamics of a physical system of two Bose-Einstein condensates, flowing in ring-shaped optical potentials, and mutually interacting through tunnel coupling. The experimental setup, provided in Fig. 1, allows us to tune the tunneling in an experimentally feasible way. The system is governed by a Bose-Hubbard two-leg ladder Hamiltonian, pierced by a synthetic magnetic field, effectively twisting the boundary conditions of the two rings. We remark that the Galilean symmetry is broken in such a system, along the ring-ring coupling direction. In the weak ring-ring coupling regime, the microscopic degrees of freedom (the phase slips between adjacent wells along the rings) are integrated out, leading to an effective action of a two-level system for the ring-ring phase slip. This implies that such physical system provides indeed a qubit, analogous to the flux qubit built with superconductor Josephson junctions. It would be interesting to study the effective dynamics beyond the weak coupling approximation.

The real-time evolution of population imbalance and phase difference between the two flowing condensates is analyzed, through two coupled Gross-Pitaevskii equations obtained from the Bose-Hubbard ladder in the mean-field equations. The dynamics is thoroughly analyzed in the different regimes depending on the values of the s-wave scattering, tunneling rate, synthetic "magnetic fluxes," and initial population imbalances ($\lambda\rho$, g, Δ, and Z_0, respectively). It is evidenced how the macroscopic quantum self-trapping occurs in our system. It is shown that population imbalance takes values in only classically allowed regions of oscillation.

It would be interesting to describe our system including the quantum fluctuations around the mean-field solution [38,39].

ACKNOWLEDGMENTS

We thank F. Auksztol, H. Crepaz, R. Dumke, F. Hekking, A. J. Leggett, A. Minguzzi, and G. Rastelli for discussions.

APPENDIX A: PEIERLS SUBSTITUTION FOR THE BOSE-HUBBARD LADDER MODEL

In this appendix we review the "Peierls substitution" in the Bose-Hubbard ladder, corresponding to applying of two different "magnetic fluxes" to the two-ring lattice system [see Eq. (4)].

The hopping element t can be expressed through Wannier functions $\phi(\mathbf{x} - \mathbf{R}_i)$ and single-particle Hamiltonian h_1 in the subsequent form:

$$t_0 = \int dx^3 \phi^*(\mathbf{x} - \mathbf{R}_i) h_1 \phi(\mathbf{x} - \mathbf{R}_{i+1}). \tag{A1}$$

The Wannier functions $\phi(\mathbf{x} - \mathbf{R}_i)$ are localized around $\mathbf{R}_i$ lattice sites. In the absence of "electromagnetic fields" the single-particle Hamiltonian is given by

$$h_1 = \frac{\mathbf{p}^2}{2m} + V(\mathbf{x}), \tag{A2}$$

where the first term is kinetic energy and second term is a one-body potential energy. Once the synthetic gauge field $\mathbf{A}(\mathbf{x},t)$ is generated we can take it into account by substitution $\mathbf{p} \to \mathbf{p} - \mathbf{A}(\mathbf{x},t)$ in the single-particle Hamiltonian. We can rewrite the hopping element in the presence of the synthetic gauge field in the following form:

$$t = \int dx^3 \tilde{\phi}^*(\mathbf{x} - \mathbf{R}_i) h_1 \tilde{\phi}(\mathbf{x} - \mathbf{R}_{i+1}), \tag{A3}$$

where $\tilde{\phi}(\mathbf{x}-\mathbf{R}_i) = e^{-i\Lambda(\mathbf{x},t)}\phi^*(\mathbf{x}-\mathbf{R}_i)$ with $\Lambda(\mathbf{x},t) = \int_{\mathbf{x}_0}^{\mathbf{x}} \mathbf{A}(\mathbf{x},t)\mathbf{dx}$, where $\mathbf{x}_0$ is an arbitrary point. Assuming that $\mathbf{A}(\mathbf{x},t)$ is a slowly varying function on an atomic scale,

$$\tilde{\phi}(\mathbf{x}-\mathbf{R}_i) \approx e^{-i\Lambda(\mathbf{R}_i,t)}\phi^*(\mathbf{x}-\mathbf{R}_i), \tag{A4}$$

By substituting Eq. (A4) in Eq. (A3) we finally get

$$t = e^{i\Phi}t_0, \;\; \Phi = \int_{\mathbf{R}_i}^{\mathbf{R}_{i+1}} \mathbf{A}(\mathbf{x},t)\mathbf{dx}. \tag{A5}$$

The idea, that all the effect of electromagnetic field in the lattice can be absorbed in the hopping matrix element is called Peierls substitution. We would like to emphasize that the inter-ring hopping element g is not affected by the Peierls substitution because the synthetic gauge field is assumed to have components longitudinal to the rings only.

APPENDIX B: SOLUTION IN TERMS OF ELLIPTIC FUNCTIONS

As it was shown in Sec. IV, the dynamics of the population imbalance and the phase difference of the condensates in the two coupled rings is given by

$$\frac{\partial Z}{\partial \tilde{s}} = -\sqrt{1-Z^2}\sin\Theta, \tag{B1}$$

$$\frac{\partial \Theta}{\partial \tilde{s}} = \Delta + \lambda\rho Z + \frac{Z}{\sqrt{1-Z^2}}\cos\Theta. \tag{B2}$$

In this appendix we discuss the analytical solutions of the equations above, for the two different cases: $\Delta = 0$ and $\Delta \neq 0$.

Equations (B1) and (B2) can be derived from the Hamiltonian,

$$\begin{aligned} H(Z(\tilde{s}),\Theta(\tilde{s})) &= \frac{\lambda\rho Z^2}{2} + \Delta Z - \sqrt{1-Z^2}cos\Theta \\ &= H_0, \end{aligned} \tag{B3}$$

where Z and Θ are canonically conjugate variables. Indeed, $H(Z(t),\Theta(t)) = H(Z(0),\Theta(0)) = H_0$ because the energy of the system is conserved. Combining Eqs. (B1) and (B3) Θ can be eliminated, obtaining

$$\dot{Z}^2 + \left[\frac{\lambda\rho Z^2}{2} + \Delta Z - H_0\right]^2 = 1 - Z^2, \tag{B4}$$

that is solved by quadratures:

$$\frac{\lambda\varrho\tilde{s}}{2} = \int_{Z(0)}^{Z(\tilde{s})} \frac{dZ}{\sqrt{f(Z)}}, \tag{B5}$$

where $f(Z)$ is the following quartic equation,

$$f(Z) = \left(\frac{2}{\lambda\rho}\right)^2(1-Z^2) - \left[Z^2 + \frac{2Z\Delta}{\lambda\rho} - \frac{2H_0}{\lambda\rho}\right]^2. \tag{B6}$$

There are two different cases: $\Delta = 0$ and $\Delta \neq 0$.

(I.) $\Delta = 0$. In this case the solution for the $Z(t)$ can be expressed in terms of "cn" and "dn" Jacobian elliptic functions as ([26])

$$\begin{aligned} Z(\tilde{s}) &= Ccn[(C\lambda\rho/k(\tilde{s}-\tilde{s}_0),k)] \;\; for \;\; 0<k<1 \\ &= C\,\mathrm{sech}(C\lambda\rho(\tilde{s}-\tilde{s}_0)), \;\; for \;\; k=1 \\ &= Cdn[(C\lambda\rho/k(\tilde{s}-\tilde{s}_0),1/k)] \;\; for \;\; k>1; \end{aligned} \tag{B7}$$

$$k = \left(\frac{C\lambda\rho}{\sqrt{2}\zeta(\lambda\rho)}\right)^2 = \frac{1}{2}\left[1 + \frac{(H_0\lambda\rho - 1)}{(\lambda\rho)^2 + 1 - 2H_0\lambda\rho}\right], \tag{B8}$$

where

$$\begin{aligned} C^2 &= \frac{2}{(\lambda\rho)^2}((H_0\lambda\rho - 1) + \zeta^2), \\ \alpha^2 &= \frac{2}{(\lambda\rho)^2}(\zeta^2 - (H_0\lambda\rho - 1)), \\ \zeta^2(\lambda\rho) &= 2\sqrt{(\lambda\rho)^2 + 1 - 2H_0\lambda\rho}, \end{aligned} \tag{B9}$$

and $\tilde{s}_0$ fixing $Z(0)$. Jacobi functions are defined in terms of the incomplete elliptic integral of the first kind $F(\phi,k) = \int_0^\phi d\theta(1-k\sin^2\theta)^{-1/2}$ by the following expressions: $sn(u|k) = \sin\phi, cn(u|k) = \cos\phi$, and $dn(u|k) = (1-k\sin^2\phi)^{1/2}$ [40]. The Jacobian elliptic functions $sn(u|k)$, $cn(u|k)$, and $dn(u|k)$ are periodic in the argument u with period $4K(k)$, $4K(k)$, and $2K(k)$, respectively, where $K(k) = F(\pi/2,k)$ is the complete elliptic integral of the first kind. For small elliptic modulus $k \simeq 0$ such functions behave as trigonometric functions; for $k \simeq 1$ they behave as hyperbolic functions. Accordingly, the character of the solution of Eqs. (B1) and (B2) can be oscillatory or exponential, depending on k. For $k \ll 1$, $cn(u|k) \approx \cos u + 0.25k(u - \sin(2u)/2)\sin u$ is almost sinusoidal and the population imbalance is oscillating around zero average value. When k increases, the oscillations become nonsinusoidal and for $1-k \ll 1$ the time evolution is nonperiodic: $cn(u|k) \approx \sec u - 0.25(1-k)(\sinh(2u)/2 - u)\tanh u \sec u$. From the last expression we can see that at $k=1$, $cn(u|k) = \sec u$ so oscillations are exponentially suppressed and $Z(\tilde{s})$ taking 0 asymptotic value. For the values of the $k>1$ such that $[1-1/k] \ll 1$ and $Z(s)$ is still nonperiodic and is given by $dn(u|1/k) \approx \sec u + 0.25(1-1/k)(\sinh(2u)/2 + u)\tanh u \sec u$. Finally when $k \gg 1$ then the behavior switches to sinusoidal again, but $Z(\tilde{s})$ does oscillates around a nonzero average: $dn(u|1/k) \approx 1 - \sin^2 u/2k$. This phenomenon accounts for the MQST.

The periods of oscillations in the regimes considered above result to be

$$\begin{aligned} \tau &= \frac{4kK(k)}{C\lambda\rho} \;\; \text{for} \;\; 0<k<1, \\ &= \log(4/\sqrt{1-k}) \;\; \text{for} \;\; k=1, \\ &= \frac{2K(1/k)}{C\lambda\rho} \;\; \text{for} \;\; k>1. \end{aligned} \tag{B10}$$

For $k \to 1$ the period becomes infinite and diverging logarithmically.

(II.) $\Delta \neq 0$. In this case $Z(s)$ is expressed in terms of the Weierstrass elliptic function ([24,26]):

$$Z(\tilde{s}) = Z_1 + \frac{f'(Z_1)/4}{\varrho(\frac{\lambda\rho}{2}(\tilde{s}-\tilde{s}_0); g_2, g_3) - \frac{f''(Z_1)}{24}}, \tag{B11}$$

where $f(Z)$ is given by an expression (B6), Z_1 is a root of quartic $f(Z)$ and $\tilde{s}_0 = (2/\lambda\rho)\int_{Z_1}^{Z(0)} \frac{dZ'}{\sqrt{f(Z')}}$. For $\sin\Theta_0 = 0$ (which is the case discussed in the text), $Z_1 = Z_0$ and consequently $s_0 = 0$. The Weierstrass elliptic function can be given as the inverse of an elliptic integral $\varrho(u; g_2, g_3) = y$,

where

$$u = \int_y^\infty \frac{ds}{\sqrt{4s^3 - g_2 s - g_3}}. \tag{B12}$$

The constants g_2 and g_3 are the characteristic invariants of ϱ:

$$\begin{aligned} g_2 &= -a_4 - 4a_1a_3 + 3a_2^2, \\ g_3 &= -a_2a_4 + 2a_1a_2a_3 - a_2^3 + a_3^2 - a_1^2a_4, \end{aligned} \tag{B13}$$

where the coefficients a_i, where $i = 1,..,4$, are given as

$$\begin{aligned} a_1 &= -\frac{\Delta}{\lambda\rho}; \quad a_2 = \frac{2}{3(\lambda\rho)^2}(\lambda\rho H_0 - (\Delta^2 + 1)), \\ a_3 &= \frac{2H_0\Delta}{(\lambda\rho)^2}; \quad a_4 = \frac{4(1 - H_0^2)}{(\lambda\rho)^2}. \end{aligned} \tag{B14}$$

In the present case $\Delta \neq 0$, the discriminant,

$$\delta = g_2^3 - 27g_3^2, \tag{B15}$$

of the cubic $h(y) = 4y^3 - g_2y - g_3$ governs the behavior of the Weierstrass elliptic functions (we contrast with the case $\Delta = 0$, where the dynamics is governed by the elliptic modulus k).

At first we consider the case $\delta = 0$.

If $g_2 < 0$,$g_3 > 0$ then ([40])

$$Z(\tilde{s}) = Z_1 + \frac{f'(Z_1)/4}{c + 3c\sinh^{-2}\left[\frac{\sqrt{3c}\lambda\rho}{2}(\tilde{s} - \tilde{s}_0)\right] - \frac{f''(Z_1)}{24}}. \tag{B16}$$

Namely, the oscillations of Z are exponentially suppressed and the population imbalance decay (if $Z_0>0$) or saturate (if $Z_0<0$) to the asymptotic value given by $Z(\tilde{s}) = Z_1 + \frac{f'(Z_1)/4}{c - f''(Z_1)/24}$.

If $g_2 > 0$, $g_3 > 0$ then ([40])

$$Z(\tilde{s}) = Z_1 + \frac{f'(Z_1)/4}{-c + 3c\sin^{-2}\left[\frac{\sqrt{3c}\lambda\rho}{2}(\tilde{s} - \tilde{s}_0)\right] - \frac{f''(Z_1)}{24}}, \tag{B17}$$

where $c = \sqrt{g_2/12}$. We see that the population imbalance oscillates around a nonzero average value $\overline{Z} \doteq Z_1 + \frac{f'(Z_1)/4}{2(2c - f''(Z_1)/24)}$, with frequency $\omega = 2g\sqrt{3c}\lambda\rho$.

We express the Weierstrass function in terms of Jacobian elliptic functions. This leads to significant simplification for the analysis of these regimes.

For $\delta > 0$, it results

$$Z(\tilde{s}) = Z_1 + \frac{f'(Z_1)/4}{e_3 + \frac{e_1 - e_3}{sn^2[\frac{\lambda\rho\sqrt{e_1 - e_3}}{2}(\tilde{s} - \tilde{s}_0), k_1]} - \frac{f''(Z_1)}{24}}, \tag{B18}$$

where $k_1 = \frac{e_2 - e_3}{e_1 - e_3}$ and e_i are solutions of the cubic equation $h(y) = 0$. In this case the population imbalance oscillates about the average value $\overline{Z} = Z_1 + \frac{f'(Z_1)/4}{2(e_1 - f''(Z_1)/24)}$.

The asymptotics of the solution is extracted through: $k \ll 1$, $sn(u|k) \approx \sin u - 0.25k(u - \sin(2u)/2)\cos u$. When k increases oscillation starts to become nonsinusoidal and when $1 - k \ll 1$ it becomes nonperiodic and takes the form, $cn(u|k) \approx \tanh u - 0.25(1 - k)(\sinh(2u)/2 - u)\sec^2 u$.

For $\delta < 0$ the following expression for $Z(s)$ is obtained:

$$Z(\tilde{s}) = Z_1 + \frac{f'(Z_1)/4}{e_2 + H_2\frac{1 + cn[\lambda\rho\sqrt{H_2}(\tilde{s} - \tilde{s}_0), k_2]}{1 - cn[\lambda\rho\sqrt{H_2}(\tilde{s} - \tilde{s}_0), k_2]} - \frac{f''(Z_1)}{24}}, \tag{B19}$$

where $k_2 = 1/2 - \frac{3e_2}{4H_2}$ and $H_2 = \sqrt{3e_2^2 - \frac{g_2}{4}}$. The asymptotical behavior of the function $cn(u|k)$ has been discussed in the previous subsection. As it it seen from this expression $Z(\tilde{s})$ oscillates about the average value $\overline{Z} = Z_1 + \frac{f'(Z_1)/4}{2(e_2 - f''(Z_1)/24)}$.

The period of the oscillations of the $Z(\tilde{s})$ in this case is given by

$$\begin{aligned} \tau &= \frac{K(k_1)}{\lambda\rho\sqrt{e_1 - e_3}} \ \textit{for} \ \ \delta > 0, \\ &= \frac{K(k_2)}{\lambda\rho\sqrt{H_2}} \ \textit{for} \ \ \delta < 0. \end{aligned} \tag{B20}$$

The inter-ring tunneling Josephson current is given by

$$I = \frac{\dot{Z}N_T}{2} = I_0\sqrt{1 - Z^2}\sin\Theta. \tag{B21}$$

[1] I. Bloch, Nature (London) **453**, 1016 (2008).

[2] I. Bloch, J. Dalibard, and W. Zwerger, Rev. Mod. Phys. **80**, 885 (2008).

[3] M. Saffman, T. G. Walker, and K. Molmer, Rev. Mod. Phys. **82**, 2313 (2010).

[4] G. Raithel, G. Birkl, A. Kastberg, W. D. Phillips, and S. L. Rolston, Phys. Rev. Lett. **78**, 630 (1997); S. E. Hamann, D. L. Haycock, G. Klose, P. H. Pax, I. H. Deutsch, and P. S. Jessen, *ibid.* **80**, 4149 (1998), and references therein.

[5] S. Friebel, C. D'Andrea, J. Walz, M. Weitz, and T. W. Hänsch, Phys. Rev. A **57**, R20 (1998).

[6] M. Raizen, C. Salomon, and Q. Niu, Phys. Today **50**, 30 (1997).

[7] L. Guidoni and P. Verkerk, Phys. Rev. A **57**, R1501 (1998), and references therein.

[8] K. I. Petsas, A. B. Coates, and G. Grynberg, Phys. Rev. A **50**, 5173 (1994).

[9] G. K. Brennen, C. M. Caves, P. S. Jessen, and I. H. Deutsch, Phys. Rev. Lett. **82**, 1060 (1999).

[10] R. Feynman, Int. J. Theor. Phys. **21**, 467 (1982).

[11] L. Amico, A. Osterloh, and F. Cataliotti, Phys. Rev. Lett. **95**, 063201 (2005).

[12] S. Franke-Arnold, J. Leach, M. J. Padgett, V. E. Lembessis, D. Ellinas, A. J. Wright, J. M. Girkin, P. Ohberg, and A. S. Arnold, Opt. Express **15**, 8619 (2007).

[13] K. Henderson, C. Ryu, C. MacCormick, and M. G. Boshier, New J. Phys. **11**, 043030 (2009).

[14] L. Amico, D. Aghamalyan, H. Crepaz, F. Auksztol, R. Dumke and L.-C. Kwek, arXiv:1304.4615.

[15] K. Volke-Sepulveda and R. Jauregui, J. Phys. B **42**, 085303 (2009).

[16] K. W. Madison, F. Chevy, W. Wohlleben, and J. Dalibard, Phys. Rev. Lett. **84**, 806 (2000).

[17] J. R. Abo-Shaeer, C. Raman, J. M. Vogels, and W. Ketterle, Science **292**, 476 (2001).
[18] Y.-J. Lin, R. L. Compton, K. Jimnez-Garcia, J. V. Porto, and I. B. Spielman, Nature (London) **462**, 628 (2009).
[19] Y.- J. Lin, R. L. Compton, K. Jimnez-Garcia, W. D. Phillips, J. V. Porto, and I. B. Spielman, Nature Physics **7**, 531 (2011).
[20] M. V. Berry, Proc. R. Soc. London A **392**, 45 (1984).
[21] A. V. Ponomarev, S. Denisov, and P. Hanggi, Phys. Rev. Lett. **102**, 230601 (2009); J. Comput. Theor. Nanosci. **7**, 2441 (2010).
[22] J. E. Mooij, T. P. Orlando, L. Levitov, Lin Tian, Caspar H. van der Wal, and Seth Lloyd, Science **285**, 1036 (1999).
[23] E. Paladino, Y. M. Galperin, G. Falci, and B. L. Altshuler, arXiv:1304.7925.
[24] J. D. Andersen and V. M. Kenkre, Phys. Rev. B **47**, 11134 (1993).
[25] A. Smerzi, S. Fantoni, S. Giovanazzi, and S. R. Shenoy, Phys. Rev. Lett. **79**, 4950 (1997).
[26] S. Raghavan, A. Smerzi, S. Fantoni, and S. R. Shenoy, Phys. Rev. A **59**, 620 (1999).
[27] M. Albiez, R. Gati, J. Fölling, S. Hunsmann, M. Cristiani, and M. K. Oberthaler, Phys. Rev. Lett. **95**, 010402 (2005).
[28] G. J. Milburn, J. Corney, E. M. Wright, and D. F. Walls, Phys. Rev. A **55**, 4318 (1997).
[29] L. D. Landau, Phys. Z. Sowjetunion **3**, 664 (1933).
[30] K. V. Sepulveda, V. G. Chavez, S. C. Cerda, J. Arlt, and K. Dholakia, J. Opt. B **4**, S52 (2002).
[31] See, for example, K. Bongs, S. Burger, S. Dettmer, D. Hellweg, J. Arlt, W. Ertmer, and K. Sengstock, Phys. Rev. A **63**, R031602 (2001).
[32] T. C. Li, H. Kelkar, D. Medellin, and M. G. Raizen, Opt. Express **16**, 5468 (2008).
[33] H. J. Schulz and B. S. Shastry, Phys. Rev. Lett. **80**, 1924 (1998); A. Osterloh, L. Amico, and U. Eckern, Nucl. Phys. B **588**, 531 (2000).
[34] R. Feynman and A. Hibbs, *Quantum Mechanics and Path Integrals* (McGraw-Hill, New York, 1965).
[35] R. Fazio and H. van der zant, Phys. Rep. **355**, 235 (2001).
[36] G. Rastelli, I. M. Pop, and F. W. J. Hekking, Phys. Rev. B **87**, 174513 (2013).
[37] A. O. Caldeira and A. J. Leggett, Phys. Rev. Lett. **46**, 211 (1981).
[38] A. Reinhard, J.-F. Riou, L. A. Zundel, D. S. Weiss, S. Li, A. M. Rey, and R. Hipolito, Phys. Rev. Lett. **110**, 033001 (2013).
[39] Shuming Li, Salvatore R. Manmana, Ana Maria Rey, R. Hipolito, A. Reinhard, J.-F. Riou, L. A. Zundel, and D. S. Weiss, arXiv:1305.4442.
[40] *Handbook of Mathematical Functions*, edited by M. Abramowitz and I. A. Stegun (Dover, New York, 1970).